Pattern formation in a gene network model with boundary shape dependence

Luis Diambra* and Luciano da Fontoura Costa†
Institute of Physics at São Carlos, University of São Paulo, Caixa Postal 369, cep 13560-970, São Carlos, SP, Brazil
(Received 30 March 2005; revised manuscript received 3 October 2005; published 20 March 2006)

A fundamental task in developmental biology is to identify the mechanisms which drive morphogenesis. Traditionally pattern formation have been modeled mainly using Turing-type mechanisms, where complex patterns arise by symmetry breaking. However, there is a growing experimental evidence that the influence of signals derived from surrounding tissues can contribute to the patterning processes. In this paper, we show that the interplay between the shape of surrounding tissues and a hierarchically organized gene regulatory network can be able to induce stable complex patterns. The rise of these patterns depends strongly on the shape of the surrounding tissues.

DOI: 10.1103/PhysRevE.73.031917 PACS number(s): 87.18.Hf, 87.18.La, 87.16.−b, 87.16.Ac

I. INTRODUCTION

Developmental biology research has identified several organizing principles that contribute in an orchestrated manner to embryogenesis and organogenesis. Recently, Salazar-Ciudad *et al.* [1] have proposed a theoretical framework that classifies developmental mechanisms into three main categories: *cell autonomous, inductive*, and *morphogenetics*. Cell autonomous development mechanisms are mainly based on cell division that occurs coupled to internal dynamics rather than to environmental signals (e.g., somitogenesis [2]). Inductive mechanisms are those in which the cells secrete diffusible molecules, as signaling, which induce changes in the states of other cells [3]. Thus, inductive patterns are determined by the spatial relationships of different cell states (phenotypes). Last but not least, morphogenetic-based mechanisms are those in which the pattern is a consequence of mechanical cell interactions (apoptosis, cell migration, differential adhesion, etc.) rather than cell states (see, e.g., [4–6]).

Since 1952, when Alan Turing showed a pathway to pattern formation without pre-patterns for its initiation [7], the literature on modeling inductive pattern formation has been mainly based on the reaction-diffusion theory of morphogens (see, for example, [8,9]). Morphogens are signaling molecules that can induce or not different cell states depending on the morphogen concentration [10,11]. Typically, a morphogen is produced by a distinct localized set of cells that diffuse to surrounding tissues generating a graded distribution across a field of cells. Thus the local concentration of this molecule would induce the state of nearby cells in a position-dependent manner. The Turing-type inductive mechanism can be thought of as a competition between activation by a slow diffusing chemical and inhibition by a faster chemical, and has been largely applied to explain biological pattern formation (e.g., [8]). However, it is important to keep in mind that biological strategies of patterning can be very different from the Turing-type mechanisms where diffusion plays a key role in the symmetry-breaking. For example, the formation of the characteristic periodic striped pattern of the pair-rule expression in Drosophila [12,13] follows a strategy based on a hierarchical regulatory gene network embedded in morphogenic fields. In this example, each stripe results almost independently of each other as a consequence of the positional information provided by the spatial distribution of proteins encoded in the gap genes group, which in turn follow the positional cue provided by maternal factors. We define hierarchical gene regulatory networks as those in which the production rates of the proteins associated with the higher-level genes are not affected by the gene product of the lower-level genes, whose expression is regulated by the higher level genes. Hereafter, we will refer to the strategy based on a hierarchically regulatory gene network as *hierarchic-type strategy*. This type of strategy differs from the Turing-type in that the diffusion constants associated with the morphogens are not required to be different for the pattern formation. However, the extent to which the patterns under development are Turing-type or hierarchic-type remains an unsolved issue [14–16].

In general, inductive mechanisms act under the influence of tissues whose form is subjected to morphogenetics mechanisms. On the other hand, molecular signaling underlying inductive patterns can activate or not, depending on its local concentration, morphogenetics mechanisms which in turn act over the inductive mechanisms themselves. Thus, the shape of organ and tissues could often be the outcome of the inductive-morphogenetics mechanisms interacting reciprocally in a continuous and concerted manner. Salazar-Ciudad *et al.* named this synergetic activity *morphodynamic* interaction [1,17]. Consequently, when inductive and morphogenetic mechanisms interact, the space in which diffusion takes place changes over time, affecting the inductive patterning process. Depending on the temporal order in which each mechanism acts, or the typical timing involved in each mechanism, it is possible in some cases to consider a one-way interaction. In this sense, Salazar-Ciudad *et al.* refer to *morphostatic* interaction, when morphogenetics mechanisms act after the inductive pattern formation [1]. In the same

*Author to whom all correspondence should be addressed. Present address: Instituto de Pesquisa e Desenvolvimento, Universidade do Vale do Paraíba, Caixa Postal 8088, cep 12244-000, São Jose dos Campos SP, Brazil. Electronic address: diambra@univap.br
†Electronic address: luciano@if.sc.usp.br

spirit, one could approximate by a one-way interaction those cases in which the typical morphogenetics timings are larger than the typical time of the inductive pattern formation. Hereafter, we denoted this approximation as morphostatic approximation.

In most cases, the shape of endogenous morphogen gradients is rarely known. Only a few systems have been studied intensively to identify the appropriate morphogens and their associated spatial distribution. Furthermore, the regulatory gene networks, as well as the signaling pathway involved in developmental programs, are not, in most cases, quantitatively characterized. For these reasons, we use mathematical modeling to explore the hierarchic-type inductive mechanisms as a putative generic mechanisms for complex pattern formation rather than modeling a particular developing biological system. However, there exists much experimental evidence for our modeling. For example, in Xenopus embryos, it has been established that bone morphogenetic protein controls neural and epidermal fates in the vertebrate ectoderm, under the control of antagonists secreted by the organizer region of the mesoderm [18]. Also wingless, hedgehog, and decapentaplegic proteins in the Drosophila wing imaginal disks are well studied examples of secreted signaling proteins [19]. Furthermore, BMP4 evokes distinct responses in ectodermal cells at high and low concentrations, in a pattern that is consistent with the positions of the corresponding cell types in the Xenopus embryo [20]. Recently, Miyazaki *et al.* showed that the morphogenesis of a mouse embryonic submandibular gland depends (SMG) on intraepithelial signaling mediated by an epidermal growth factor, and on the neuregulin-1 protein, which is exclusively found in the mesenchyme. Their result suggests that both mesenchyme-derived molecules and epithelium-derived molecules drive the SMG morphogenesis [21].

Modeling pattern formation is a current research topic in developmental biology. Recently, several studies have considered the effects of curvature and growth constraint on pattern formation [22–24]. There is also literature considering particular developing systems such as stripe formation in Pomacanthus including cell migration [9], mammalian teeth using the morphodynamic approach [25], the segment polarity network in Drosophila [3], and limb bud patterning including growth [26]. Most of these works have used Turing-type mechanisms for modeling. In this paper, we focus on some aspects of hierarchic-type inductive mechanisms within the morphostatic approximation. In particular, we will explore, by means of computational simulations, the ability of a small gene regulatory network to form complex patterns by the influence of different shapes of morphogen sources. The gene network studied is able to generate stable complex patterns depending on the shape of the surrounding morphogen sources.

II. METHODS

A. Shaping morphogen gradients

Although pattern formation is indeed induced by graded activation of a signaling pathway, several factors are involved in the distribution of a morphogen in a developmental field [27]. The mechanisms involved in gradient shaping include passive diffusion in the extracellular matrix [28], repeated rounds of endocytosis and exocytosis [29], cytonemes [30], argosomes [31], and a recently proposed mechanism by mRNA decay in growing structures [32]. It is beyond the scope of this paper to model the shape gradient genesis. We will adopt the simple localized source-dispersed sink models, where the shape of a morphogen gradient is dictated by the rate of diffusion away from the site of synthesis, along with the rate degradation. The gradient can be broadened by either increasing the diffusion rate or decreasing the degradation rate, while the opposite effects can produce a much steeper gradient. In particular, the diffusive substances are homogeneously secreted by the fixed boundary of surrounding tissues. Thus, we also consider that these substances are degraded over all developmental fields. We can represent these processes by the following equations:

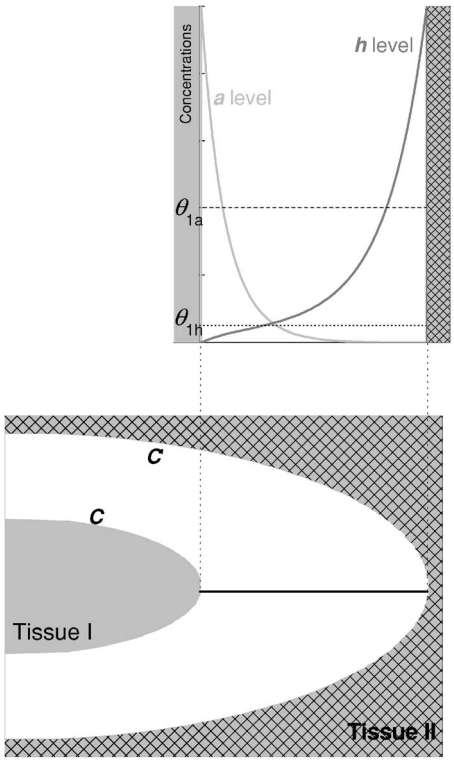

FIG. 1. A schematic representation of surrounding tissues, boundaries (bottom), and the concentration profile of activator a and inhibitor h over a horizontal segment in the middle of a semielliptic domain (top).

$$\dot{a} = D_a \nabla^2 a - \lambda_a a,$$

$$\dot{h} = D_h \nabla^2 h - \lambda_h h, \quad (1)$$

where a (h) denotes the activator (inhibitor) concentration that is released by the tissue I (tissue II) and degraded over the domain at rate λ_a (λ_h). Figure 1 shows a schematic representation of surrounding tissues, boundaries (bottom panel), and the concentration profiles a and h over a horizontal segment in the middle of a semielliptic domain (top panel).

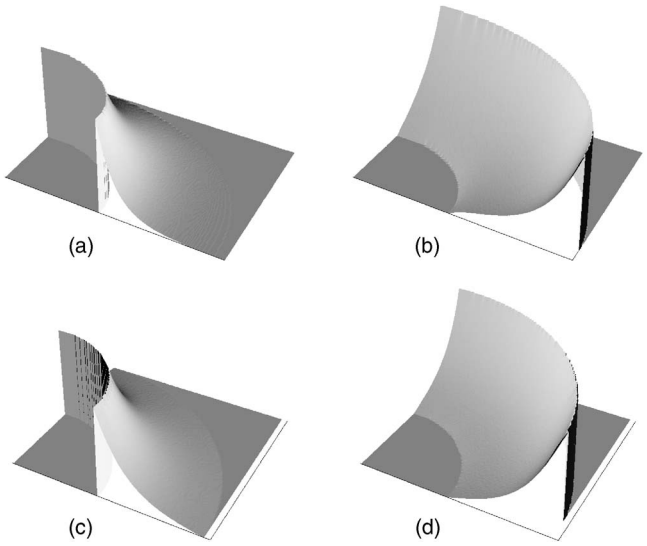

FIG. 2. 3D plots of the concentration of a, secreted by the tissue I [(a) and (c)], and h [(b) and (d)], which is secreted by the tissue II, obtained from Eqs. (1), after 5000 time steps. The panels (a) and (b) correspond to the elliptical geometry, and panels (c) and (d) correspond to the circular geometry.

In order to evidence the key role of geometrical constraints in the patterning process, the overall processes were implemented on both semielliptical and semicircular domains. Figure 2 depicts the concentration fields of activators (A) and inhibitors (B) in a portion of the semielliptical domain. For the semicircular domain, the concentration fields of activators and inhibitors are shown in (A) and (B), respectively, and they were obtained using the parameters in Table I. Despite the small differences between the top and bottom morphogen distributions, they are sufficient to induce completely different patterns of expression of regulated genes, as we will show later.

B. Gene network model for development

Our gene network model is based on a well-known biological dynamics of development: the Drosophila segmentation. This is an example in which biological strategies of patterning seem to follow a hierarchically organized building strategy defined by small modular regulatory gene networks. In this case, a concentration-dependent transcriptional activator Bicoid (Bcd) starts a regulatory cascade activating the expression of hunchback, other gap genes (Kruppel, knirps, giant, tailless), which are mutually repressed, and the pair-rule genes (e.g., eve-skipped). We have constructed a small regulatory network (see Fig. 3) whose topology mimics the Drosophila segmentation network in many aspects. For example, the higher-level gene U_1 corresponds to a concentration-dependent transcriptional activator, while U_{1-3} form the mutual inhibitor subnetwork (like the gap genes), and finally, the lower-level gene U_5 corresponds to the network output (like the pair-rule genes). This network is able to produce boundary-dependent complex patterns from an initially homogeneous distribution. Note that this result is not specific to the particular network topology used in the model. We also verify that modified versions of this network also produce patterns in a boundary shape manner.

TABLE I. Parameter values for diffusion, degradation, and geometrical constraints used to obtain the input profiles 1 and 2. These profiles differ in the degradation values λ_a and λ_h, which were reduced to 0.5×10^{-3} to generate the input profile 2.

Parameters	Values	Parameters	Values
d_i	0.01	Semiellipse	
λ_i $(i\neq5)$	0.20	internal semimajor axis	40.00
λ_5	0.35	internal semiminor axis	14.14
D_a	0.04	external semimajor axis	86.60
D_h	0.04	external semiminor axis	31.62
λ_a	1.0×10^{-3}	Semicircular	
λ_h	1.0×10^{-3}	internal radius	24.70
Δt	1.00	external radius	51.96
Δx	0.40		

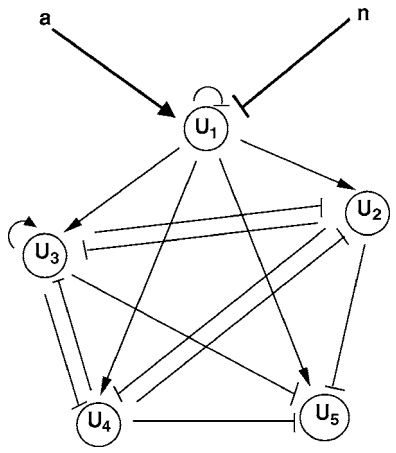

FIG. 3. Schematic diagram of the network. Circles indicate genes, blunt-end arrows denote inhibition, and pointed arrows denote activation. Regulatory activation is represented by arrows and regulatory inhibition by small perpendicular edges, as usually. This network presents two negative feedback loops, one where U2 inhibits U3 that inhibits U4 that inhibits U2, and another which is formed by U4 that inhibits U3 that inhibits U2 that inhibits U4. There is also an autoinhibitory loop acting over U1 and an autocatalytic loop acting over U2.

Our mathematical model considers several biochemical and biophysical processes currently present in many biological descriptions, including diffusion, degradation, noise, and of course, regulatory activation and/or repression of gene expressions. The last one forms two negative feedback loops, which seem to be essential control mechanisms in developmental networks [16]. We will describe regulatory activation sigmoidal functions $s^+(x,\theta,n)=x^n/(x^n+\theta^n)$. If the concentration of the activator factor is below the threshold θ, the gene is poorly expressed, whereas above this threshold its expression grows until saturation. The regulatory inhibition will be represented by $s^-=\theta^n/(x^n+\theta^n)\equiv1-s^+$. Sigmoidal functions, in particular Hill functions, have been used in a variety of genetic regulatory models [3,33–35]. In general, there are

TABLE II. Parameter values of the gene network used to obtain the pattern shown in Fig. 4. These values were also used in other simulations whenever we have not stated otherwise (see also Table III).

Parameters	Values	Parameters	Values
r_1	6.25	r_4	5.8×10^{-2}
θ_{1a}	0.40	θ_{41}	0.40
θ_{1h}	0.05	θ_{42}	0.25
θ_{11}	0.20	θ_{43}	0.20
n_{1a}	1.00	n_{41}	4.00
n_{1h}	3.00	n_{42}	2.00
n_{11}	5.00	n_{43}	2.00
r_{21}	8.06×10^{-2}	r_5	20/27
θ_{21}	1.05	θ_{51}	0.55
θ_{23}	0.35	θ_{52}	0.20
θ_{24}	0.45	θ_{53}	0.30
n_{21}	4.00	θ_{54}	0.50
n_{23}	2.00	n_{51}	4.00
n_{24}	2.00	n_{52}	3.00
r_3	0.21	n_{53}	3.00
θ_{31}	0.60	n_{54}	3.00
θ_{32}	0.10	PFL parameters	
θ_{34}	0.10	r_{22}	0.00
n_{31}	4.00	θ_{22}	0.10
n_{32}	2.00	n_{22}	3.00
n_{34}	2.00		

several regulatory interactions acting over a single gene, and in these cases the resulting expression rates will be described by the product of sigmoidal functions corresponding to each interaction [36], rather than to the additive formulation used in [3,33,34]. For the sake of simplicity, our model does not consider other factors such as growth, cell division, post-transcriptional regulation, etc., and does not explicitly distinguish between genes and their products.

We will consider five genes that form a small network of interacting genes. Their product concentrations, represented by u_i with $i=1,\ldots,5$, evolve following the reaction-diffusion equations

$$\dot{u_i} = d_i\nabla^2 u_i + f_i(a,h,\{u_i\}) - \lambda_{u_i}u_i + \eta\epsilon(t)u_i, \qquad (2)$$

where f_i represents the regulatory transcription control of gene i, and λ_i is the degradation rate. The last term represents a multiplicative noise. ϵ is a random variable that is assumed uncorrelated and Gaussian distributed (null mean and variance unitary). η represents the intensity of noise. For small values of variables u_i, the noise perturbation is also small but it is implemented whenever $u_i \geqslant 0$. Although better schemes for incorporating noise into the models can be considered (e.g., [37]), the simpler approach adopted in this work is justified as we are mostly concerned with qualitative features.

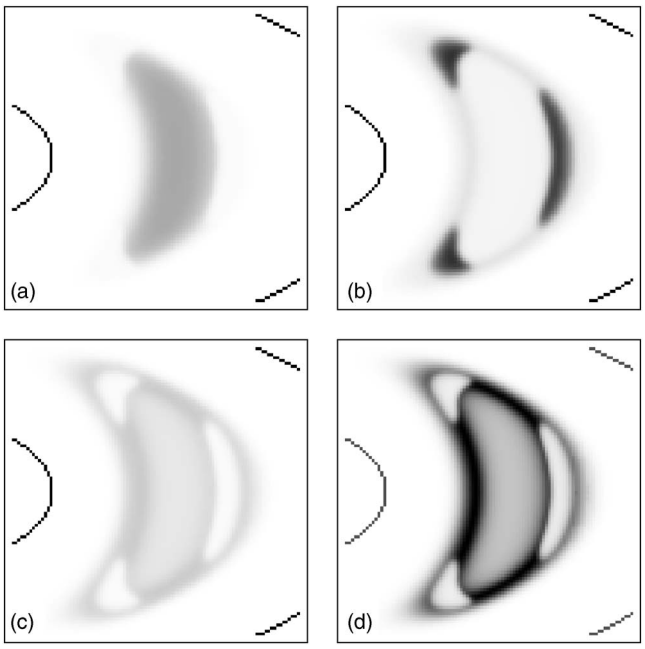

FIG. 4. Density plot of concentrations of u_2 (a), u_3 (b), u_4 (c), and u_5 (d) after 400 steps in a semielliptic domain. The model parameters used to compute these patterns are displayed in Table II.

Equation (2) governs the spatio-temporal evolution of the small regulatory gene network represented in Fig. 3. This network suffers from the influence of the surrounding tissues through the biochemical agent concentration of a and h (which are constant at a time). The particular form of f_i depends on the regulatory inputs acting over gene i, and will be discussed later.

In the hierarchically organized strategy, the regulatory role of the genes belonging to a network could be organized in different levels, for example positional level, regulatory level, output level, etc. These levels interact to constitute a specific network structure. In this framework, we can understand a complete developmental program as a network of interacting gene networks. In this spirit, the positional level will be assigned to U1, the gene associated with concentration u_1. U1 will decode the positional information derived from the geometrical constraints (boundaries) through a and h concentrations. The transcription of gene U1 will be activated when a reaches a threshold θ_{1a} and will be inhibited by h and its own product at the thresholds θ_{1h} and θ_{11}, respectively (the top panel of Fig. 1 shows the values of these parameters). Therefore, the expression of u_1 is governed by Eq. (3),

$$f_1(a,h,u_1) = r_1 s^+(a,\theta_{1a},n_{1a}) s^-(h,\theta_{1h},n_{1h}) \times s^-(a,\theta_{2a},n_{2a}). \qquad (3)$$

The expression of U1 activates in a concentration-dependent manner the genes U2, U3, and U4 (associated with the concentrations u_2, u_3, and u_4, respectively), which constitutes essentially a regulatory level of the hierarchy. U2, U3, and U4 are activated at thresholds $\theta_{21} > \theta_{31} > \theta_{41}$, respectively, and each product inhibits the transcription of the

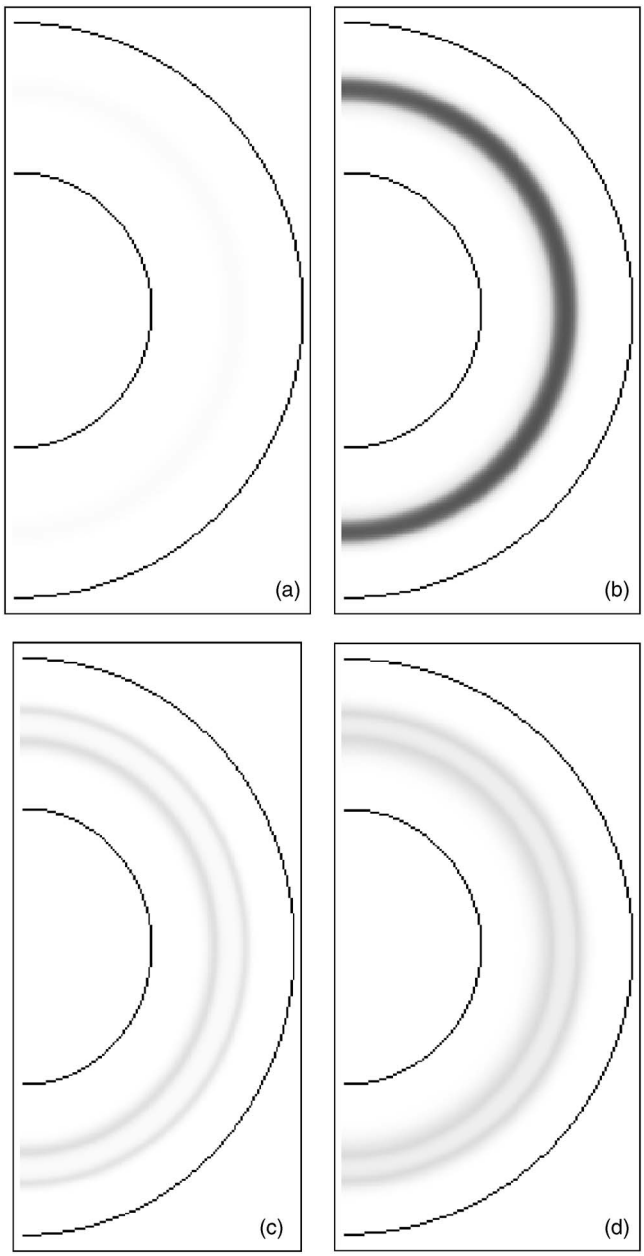

FIG. 5. Density plot of concentrations of u_2 (a), u_3 (b), u_4 (c), and u_5 (d) after 400 time steps. In this semicircular domain, no localized structure were observed for any set of parameter values.

other genes, thus forming two negative feedback loops. So, we can write

$$f_2(\{u_i\}) = r_{22}s^+(u_2,\theta_{22},n_{22}) + r_{21}s^+(u_1,\theta_{21},n_{21}) \times s^-(u_3,\theta_{23},n_{23})s^-(u_4,\theta_{24},n_{24}), \quad (4)$$

where $\{u_i\}$ represents the set of variables $\{u_1,u_2,u_3,u_4,u_5\}$. for $r_{22}>0$, this gene is also self-activated. We have added a self-activated term in Eq. (4) to study their effects over noise control,

$$f_3(\{u_i\}) = r_3s^+(u_1,\theta_{31},n_{31})s^-(u_2,\theta_{32},n_{32}) \times s^-(u_4,\theta_{34},n_{34}), \quad (5)$$

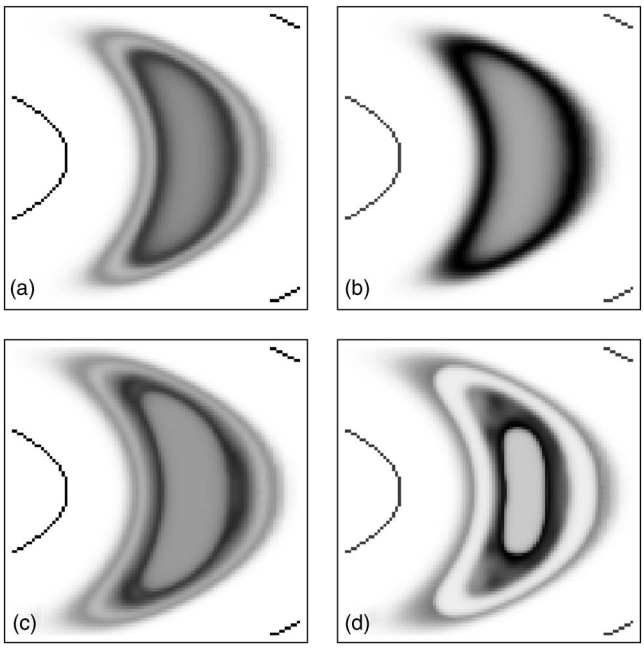

FIG. 6. Density plot of concentrations of u_5 after 400 time steps obtained for four different topologies with the network parameters displayed in Table II. The original network was modified removing the inhibitor loop $U_2 \dashv U_3 \dashv U_4 \dashv U_2$ (a), the inhibitor loop $U_4 \dashv U_3 \dashv U_2 \dashv U_4$ (b), removing the inhibitor loop $U_2 \dashv U_3 \dashv U_4 \dashv U_2$ and adding an inhibitor edge from U_5 to U_1 (c) and adding an inhibitor edge from U_5 to U_1.

$$f_4(\{u_i\}) = r_4s^+(u_1,\theta_{41},n_{41})s^-(u_2,\theta_{42},n_{42}) \times s^-(u_3,\theta_{43},n_{43}). \quad (6)$$

Thus the gradient associated with u_1 generates discrete spatial domains of regulatory factors that interact between them and generate a more complicated spatial domain of transcription of the third level of the hierarchy, the output level. For simplicity, we consider also that this level is constituted by only one gene. Its activation is promoted by u_1 and it is down-regulated by the gene products of the former level, u_2, u_3, and u_4,

$$f_5(\{u_i\}) = r_5s^+(u_1,\theta_{51},n_{51})s^-(u_2,\theta_{52},n_{52}) \times s^-(u_3,\theta_{53},n_{53})s^-(u_4,\theta_{54},n_{54}). \quad (7)$$

The positive and negative feedback loops of the model are shown in Fig. 3. It is important to keep in mind that the model was constructed to illustrate that gene networks, embedded in feedback control principles, can induce or not complex patterns depending on the boundary shape of the problem. For the aim of our study, this small network is enough. Of course, other kinds of networks can be designed to model specific developmental systems.

III. RESULTS

A. The hierarchic network strategy

The boundary problem is completely specified by Eqs. (1), the initial condition (IC), and the boundary condition

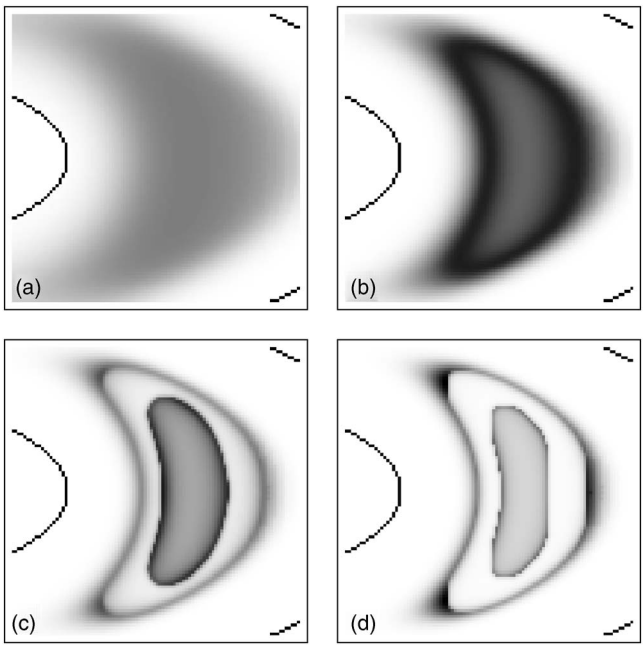

FIG. 7. Density plot of concentrations of u_5 after 400 time steps obtained for crescent values of all Hill coefficients ($n_{ij}=1$, 2, 3, and 4), while other parameter values are the same as Fig. 5.

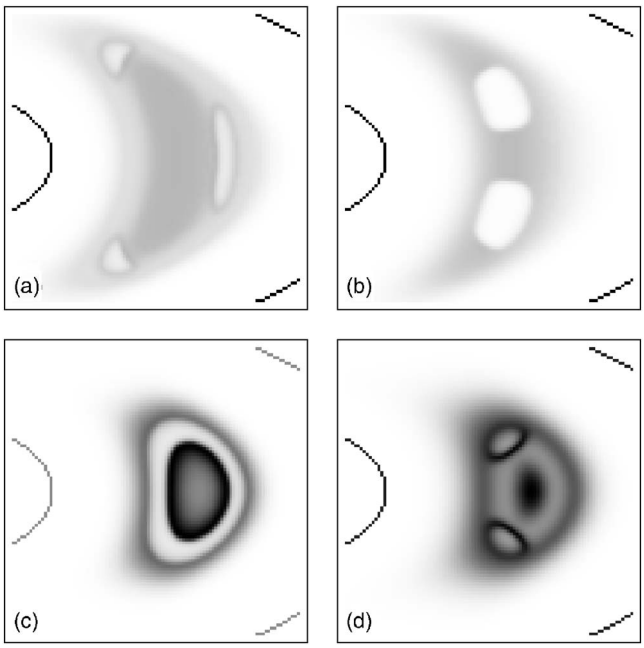

FIG. 8. Density plot of concentrations of u_5 after 400 time steps obtained for inputs profile 1 [(a) and (b)] and inputs profile 2 [(c) and (d)] with the network parameters displayed in Table III.

(BC). In this sense, when $a=1$ over C and null over C', the two vertical boundary segments are connected by a periodic boundary condition; while the inhibitor is $h=1$ over C' and null over C, the two vertical boundary segments are connected by a periodic boundary condition. Initially, both a and h concentrations are null over all domains compatible with BC. We integrate numerically Eqs. (1) for two different situations that differ in degradation parameter values. The simulations run for a long period of time (5000 steps) after which the resulting concentrations a and h are stationary. Then, these concentrations will be used as input signals acting over the network in several different conditions.

The aim of this paper is to study the effects of boundary shape on the patterning in a developmental model. For this purpose, we have elaborated a gene regulatory network model with 52 parameters, which is studied by numerical

TABLE III. Parameter values of the gene network used to obtain the patterns shown in Fig. 9. The values of parameters not shown in this table are the same as in Table II.

Figure 7(a)		Figure 7(b)		Figure 7(c)		Figure 7(d)	
Parameters	Values	Parameters	Values	Parameters	Values	Parameters	Values
r_{21}	6.85×10^{-2}	r_1	9.25	r_1	7.50	r_1	7.50×10^{-6}
θ_{21}	0.99	θ_{11}	0.265	θ_{1a}	0.20	r_{21}	8.46×10^{-2}
n_{21}	5.00	r_{21}	12.09×10^{-2}	r_{21}	12.09×10^{-2}	θ_{21}	0.95
r_3	0.215	θ_{21}	0.85	θ_{21}	1.30	n_{21}	5.00
θ_{31}	0.65	n_{21}	5.00	n_{21}	5.00	r_3	0.27
r_4	5.60×10^{-2}	r_3	32.02×10^{-2}	r_3	0.18	n_{31}	2.00
r_5	0.18	r_4	6.24×10^{-2}	r_4	5.20×10^{-2}	r_4	9.75×10^{-2}
θ_{51}	0.50	r_5	35/216	r_5	10/9	θ_{41}	0.45
θ_{52}	0.55	θ_{51}	0.50	θ_{51}	0.52	θ_{42}	0.20
θ_{53}	0.50	θ_{52}	0.40	θ_{52}	0.40	n_{41}	2.00
θ_{54}	0.20	n_{51}	2.00	θ_{53}	0.30	r_5	8.54
n_{51}	2.00			θ_{54}	0.25	θ_{51}	0.50
				n_{51}	3.00	θ_{52}	0.40
						θ_{53}	0.20
						θ_{54}	0.20
						n_{51}	2.00

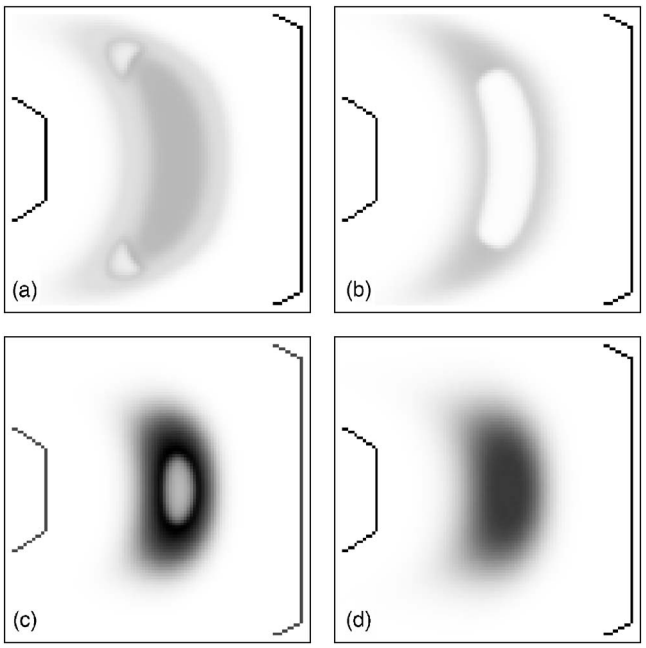

FIG. 9. Density plot of concentrations of u_5 after 400 steps obtained in the same condition as Fig. 8 with the exception in the boundary condition, which was perturbed.

simulations. Before massive computation, we need to establish some guidelines to set the parameters. The $\theta_{i,j}$ parameters represent the threshold for switching on or off the transcription processes. They were setted in the interval [0.0,1.2]. In particular, the thresholds corresponding to the activation of U2, U3, and U4 by U1 are sorted in decreasing order so as to form a sequence of activation; we set them to $\theta_{41}=0.4$, $\theta_{31}=0.6$, and θ_{21} ranges from 0.9 to 1.2. The diffusion constants and degradation rates are initially the same for all biochemical species (0.01 and 0.20, respectively). Initially, the level of noise was null for all species. Tables I and II display the parameter values used for most computations, otherwise we will mention other parameter values.

The set of partial differential equations were discretized using standard finite difference methods. The resulting large-scale dynamical system was integrated in time using forward Euler integration. We have performed simulations for different sets of parameters subject to the above-mentioned restrictions. We have found that patterns are sensitive to the spatial profile concentration of a and h and the parameters that regulate the activation and repression of U1 expression, θ_{1a}, θ_{1h}, and θ_{11}. For any given profiles a and h, there are regions in the parameter space where no patterns form, mainly due to the fact that activator concentration a does not reach the threshold θ_{1a}. An interplay of these parameters and both a and h profiles controls the position and the coarse-grain aspect of the pattern shapes.

Figure 4 depicts the density of concentrations of u_2 (A), u_3 (B), u_4 (C), and u_5 (D) obtained using the input profile 1 (see Table I) after 400 time steps, when stationarity is reached. We can see that the concentrations present complementary aspects. In general, the pattern of the output level is particularly complex as it is under the effects of four regulatory fields. In contrast, the concentration corresponding to u_2 is the simplest one because the regulatory field is almost homogeneous in its expression domain. We have observed through several simulations that these characteristics are quite general.

The remarkable observation in our study is the fact that geometrical constraints play a key role when surrounding tissues secrete morphogenic substances. Localized patterns, similar to those developed in the semielliptic domain, were not formed in a semicircular domain. In the last case, we were not able to tune the parameters in order to obtain patterns different from semicircular stripes as shown in Fig. 5. The reason for that is based on the fact that (despite the fact that diffusively substances a and h are uniformly secreted by the surrounding tissue) the curvature of the tissues is not homogeneous in the elliptic case, but it is homogeneous in the circular case. The two fronts of secreted substances are able to generate a localized expression domain for U1 in the nonhomogeneous curvature case. The striped patterns associated with semicircular domains were also found to be robust, in the sense that no abrupt changes are implied when the boundary shape changes progressively from a circle into an ellipse. The position where the complex structures appear

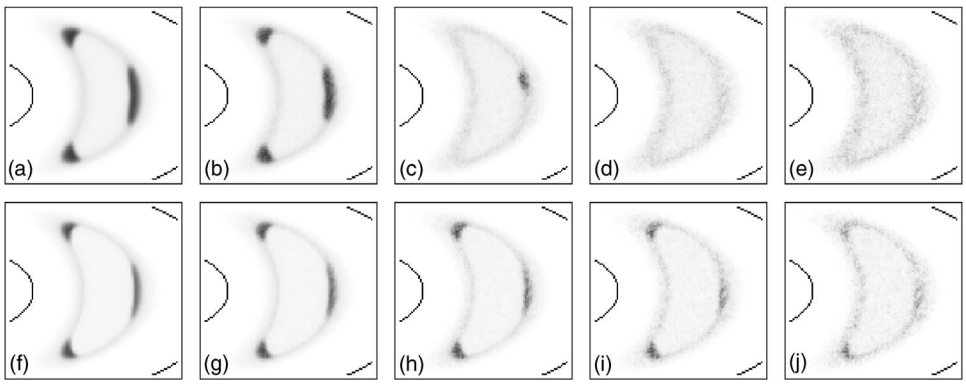

FIG. 10. Density plot of u_3 obtained, after 400 steps, when the dynamics of the gene network is perturbed with noise. The top panels correspond to patterns obtained from the network without the positive feedback loop for increasing level of noise (sorted from left to right). The bottom panels correspond to patterns obtained from the network with the feedback loop for increasing level of noise (sorted from left to right). The levels of noise used were $\eta=0.0$ [(a) and (f)], $\eta=0.05$ [(b) and (g)], $\eta=0.10$ [(c) and (h)], $\eta=0.15$ [(d) and (i)], and $\eta=0.20$ [(e) and (j)]. For further information, see the text.

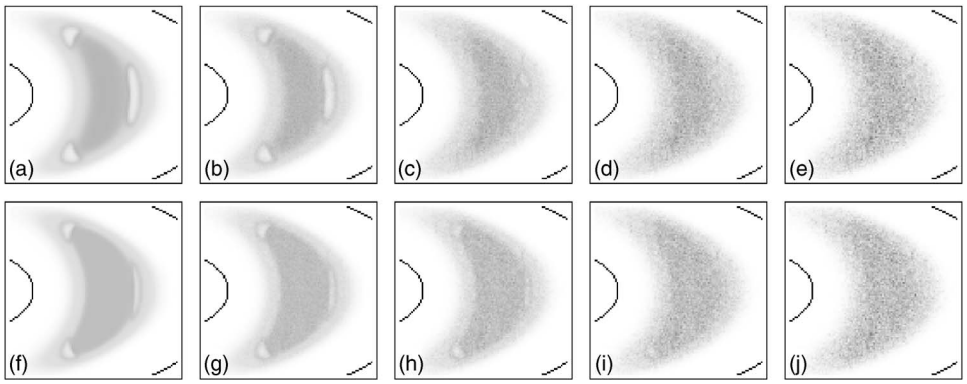

FIG. 11. Density plot corresponding to u_5 obtained in the same situation as in Fig. 10.

in Fig. 4 corresponds to the maximal value of the surrounding tissue curvature. In contrast, for homogeneous curvature the expression domains are not localized and that does not depend on tuning adequately the network parameters. We observed that the boundary shape dependence is not a property of the particular network topology by running simulations modifying the network topology. Figure 6 depicts the pattern of expression level corresponding to u_5 after 400 steps using the same parameters as in Fig. 4. In Fig. 6(a), the inhibitor loop $U_2 \dashv U_3 \dashv U_4 \dashv U_2$ was removed, while in Fig. 6(b) the inhibitor loop $U_4 \dashv U_3 \dashv U_2 \dashv U_4$ was removed. In Fig. 6(c), the original network was modified removing the inhibitor loop $U_2 \dashv U_3 \dashv U_4 \dashv U_2$ and adding an inhibitor edge from U_5 to U_1 ($\theta_{15}=0.85$, $n_{15}=3$), while in Fig. 6(d) we have only added the inhibitor edge from U_5 to U_1. Despite the fact that the four topologies present different patterns, they share the boundary shape dependence property. This result suggests that many gene networks may exhibit these properties when exposed to signaling tissues with nonhomogeneous curvature (which is normally the case in development).

In our model, the gene expression rates involve Hill functions whose coefficients $n_{i,j}$ range from 1 to 5. The case $n_{i,j}>1$ reflects the fact that *cis*-regulatory systems have usually many binding sites for each *trans*-regulatory element. These parameters can influence the shape patterns, in particular by controling the sharpness of the patterns. It is biologically relevant to determine how high the Hill coefficients must be to produce complex patterns. Figure 7 depicts the pattern of expression level corresponding to u_5 after 400 steps using the same values for all Hill coefficients in an increasing manner [$n_{i,j}=1$ (A), $n_{i,j}=2$ (B), $n_{i,j}=3$ (C), and $n_{i,j}=4$ (D) for all $n_{i,j}$]. For simplicity, all other parameter values are the same as those used in Fig. 4. It is clear from these results that low Hill coefficients are not able to generate complex patterns which became apparent for Hill coefficients greater than 3.

The same network can generate different patterns depending on the parameter values and the input profiles. Figure 8 illustrates four patterns of expression level corresponding to u_5 after 400 steps. The patterns displayed at the top (A and B

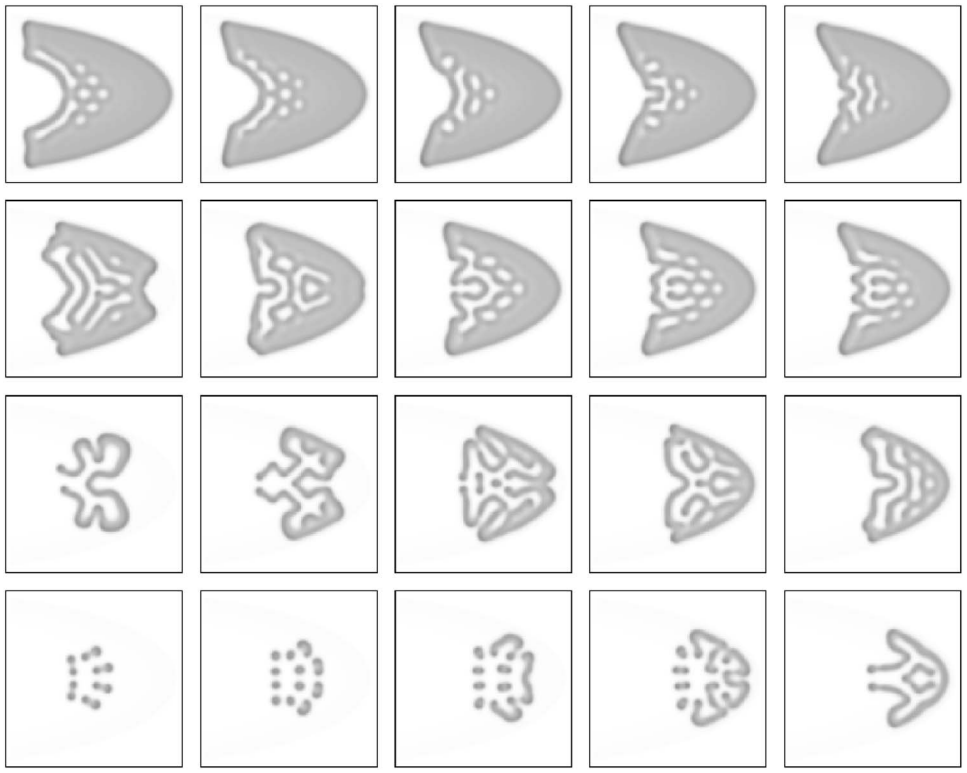

FIG. 12. Gray-Scott model in elliptic geometry: Density plot of the v concentration for different position of perturbation, increasing from left to right, and for different values of parameter k, which increases from top to bottom (see details in text).

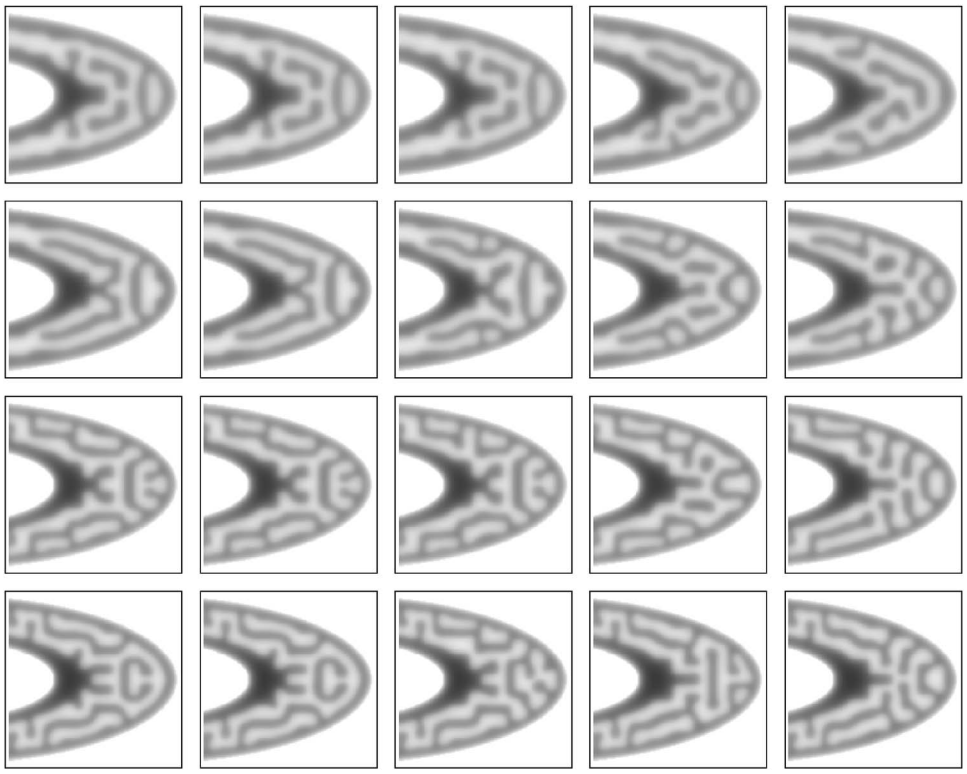

FIG. 13. MFN model in elliptic geometry: Density plot of the v concentration for different position of perturbation, increasing from left to right, and for different values of parameter k, which increases from top to bottom (see details in text).

panels) have been obtained using profiles 1 (see Table I) and two different sets of parameter values. In panel A, the system reached stationarity, while panel B reached stationarity after 800 steps (see [38]). Stationary patterns displayed at the bottom (C and D panels) have been obtained using profiles 2 (see Table I). The parameter values are shown in Table III. Often different sets of parameter values lead to the same expression pattern, but the way to reach this pattern can differ from set to set. Movie 1 illustrates the evolution of the network in two different conditions. The right panel of the movie corresponds to the same condition as in Fig. 8(b), while in the left panel we changed slightly the value of the parameter to $r_3=32.1\times10^{-2}$. Both simulations correspond to 800 steps. We can see that the final patterns are almost the same, but their temporal evolutions are quite different.

Small perturbations of boundary conditions affect the patterning processes differently, depending on the network parameters. For example, Fig. 9 shows patterns generated by the network in the same conditions as in Fig. 8, but with a perturbation in the boundary tissues (both in C and C'). The panels of Fig. 9 illustrate that the perturbation can affect a little, as in panel A, or too much, destroying completely the patterns, as in panels C and D. This result suggests that the shape of the tissue strongly influences the formation of pattern expression, and biochemical interactions are not a necessary condition to explain alterations in the resulting gene expression patterns. The influence could be through the geometrical constraint imposed by the surrounding tissues.

In general, a genetic network that underlies the developmental programs of living cells must withstand considerable random perturbations. This occurs with fluctuation in, for example, transcription, translation, and RNA and protein degradation [39,40]. We have also studied by numerical simulation the effects of the noise on the patterns in two situations. For all the previous cases we have setted $r_{22}=0.0$, i.e., there is no autocatalytic feedback acting over u_2. It would be interesting to compare the effect of noise when this positive feedback loop is present in the network. Figures 10 and 11 show the expression profiles of u_3 and u_5, respectively, obtained for five different levels of noise $\eta=0.00$ (A and F), $\eta=0.05$ (B and G), $\eta=0.10$ (C and H), $\eta=0.15$ (D and I), and $\eta=20$ (E and J). In both figures, the top panels (A–E) correspond to the network without the above-mentioned autocatalytic loop, while the bottom panels correspond to the network with the loop. The network parameter values used in both cases were the same as those used in Fig. 9(a), except for parameters r_{21} and r_{22}, which, in the case of the network with the loop, change from 6.85×10^{-2} to 4.84×10^{-2} and from zero to 4×10^{-2}, respectively. We can see that pattern structure remains almost unaltered for noise level smaller than $\sim10\%$ for the network with the autocatalytic loop. On the other hand, when this loop is absent ($r_{22}=0.0$), the patterns seem to be more noise-sensitive. This example illustrates that the particular network used is robust against a considerably high level of noise. This robustness could arise from the fact that there are two negative loops underlying the regulatory interactions.

B. The self-organized strategy

In order to study the influence of boundary shape on a self-organized system type, we have also implemented the Gray-Scott model and a modified Fitz-Hugh–Nagumo system on the semicircular and semielliptical domains.

The Gray-Scott model is a variant of the autocatalytic Selkov model of glycolysis, which corresponds to the following two irreversible reactions:

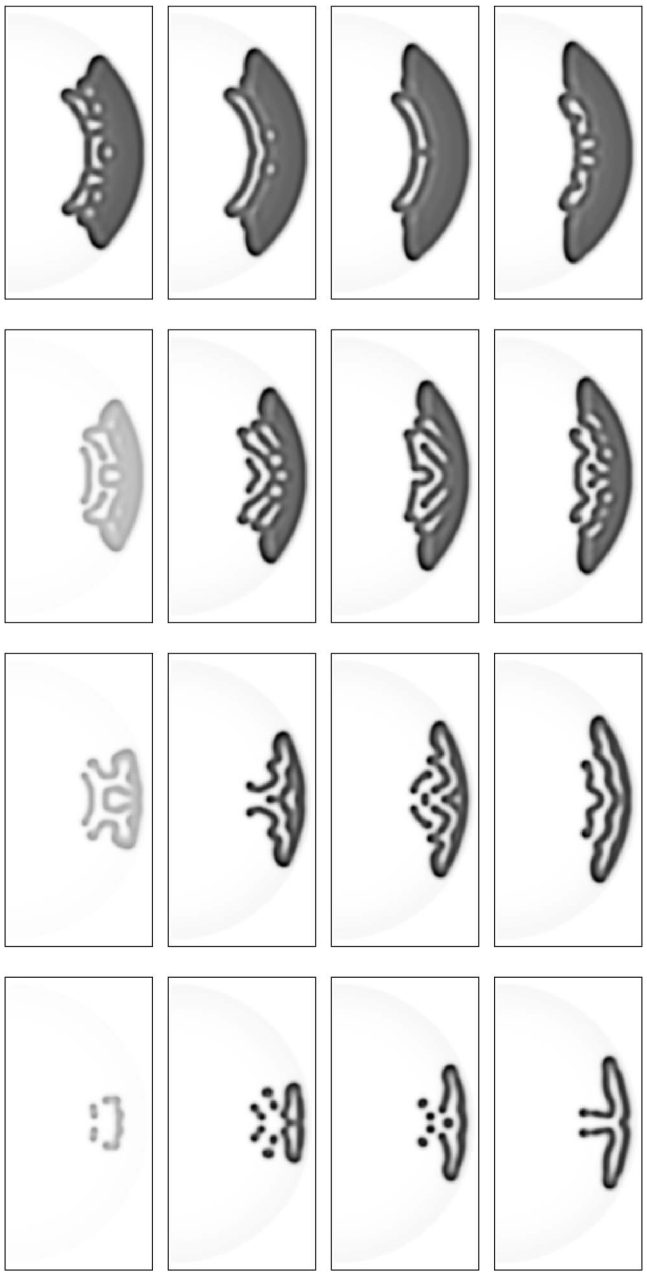

FIG. 14. Gray-Scott model in circular geometry: Density plot of the v concentration for different positions of perturbation (increasing from left to right) and for different values of parameter k (increasing from top to bottom).

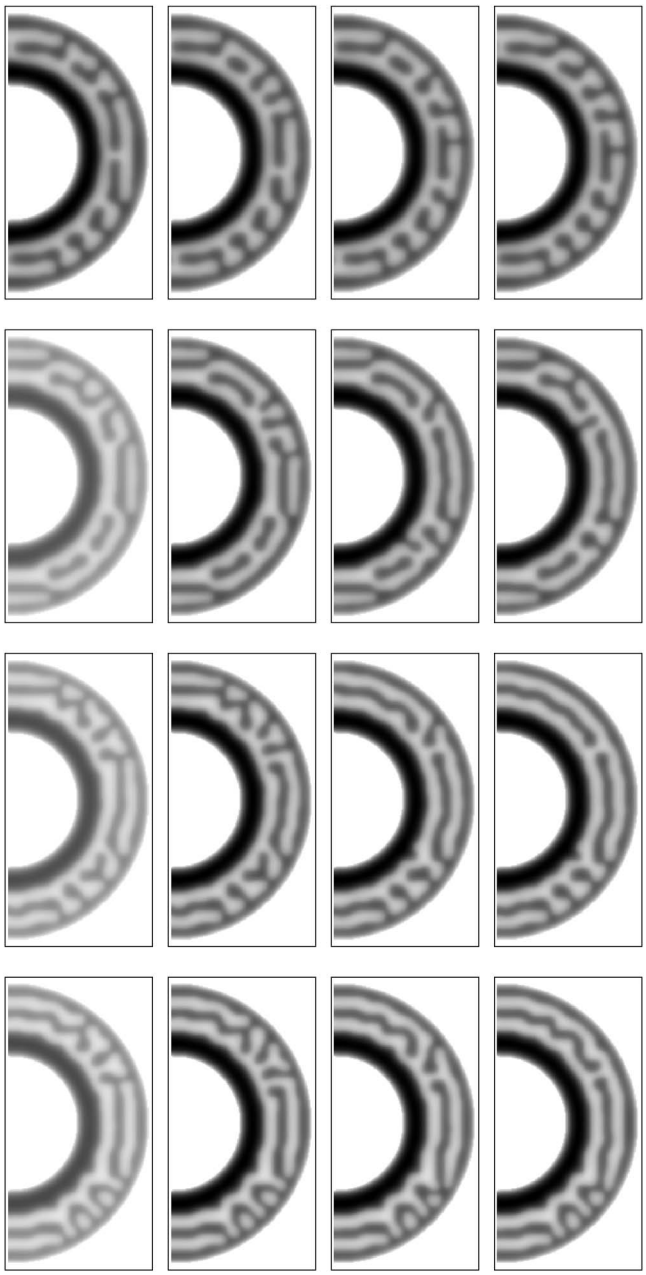

FIG. 15. MFN model in circular geometry: Density plot of the v concentration for different positions of perturbation (increasing from left to right) and for different values of parameter k (increasing from top to bottom).

$$U + 2V \rightarrow 3V,$$

$$V \rightarrow P,$$

where V catalyzes its own reaction with U, and P is an inert product. The reactor is coupled to a reservoir in which the concentrations of U and V are maintained constant. This coupling also results in both chemicals being removed from the reactor in a concentration-dependent fashion [41]. A variety of spatio-temporal patterns were derived in response to finite-amplitude perturbation [42]. We consider that u and v are coupled to the activator field a and to inhibitor h as follows:

$$\dot{u} = D_u \nabla^2 u - uv^2 + F(1-u) + r_u f(a,h),$$

$$\dot{v} = D_v \nabla^2 v + uv^2 - (F+k)v + r_v g(a,h). \quad (8)$$

We also present spatio-temporal patterns derived from a system with lateral inhibition previously study in [43],

$$\dot{u} = D_u \nabla^2 u - \alpha_1 u(u-0.05)(u-1) - v + r_u f(a,h),$$

$$\dot{v} = D_v \nabla^2 v + \alpha_2 (u-v) + r_v g(a,h). \quad (9)$$

TABLE IV. Parameter values for the Gray-Scott and MFN models.

Gray-Scott Parameters	Values	Fitz-Hugh–Nagumo Parameters	Values
F	0.04	α_1	4.50
r_u	0.002	r_u	0.305
r_v	0.004	r_v	0.00
D_u	0.0336	D_u	0.10
D_v	0.0168	D_v	0.405
$\theta_{ua}(=\theta_{uh})$	0.50	$\theta_{ua}(=\theta_{uh})$	0.08
$\theta_{va}=\theta_{vh})$	0.50	$\theta_{va}=\theta_{vh})$	
$n_{ua}(=n_{uh})$	1.0	$n_{ua}(=n_{uh})$	5.0
$n_{va}(=n_{vh})$	1.0	$n_{va}(=n_{vh})$	

Both Gray-Scott and the modified Fitz-Hugh–Nagumo (MFN) system f and g are defined by

$$f(a,h) = s^+(a,\theta_{u,a},n_{u,a})s^-(h,\theta_{u,h},n_{u,h}),$$

$$g(a,h) = s^+(a,\theta_{v,a},n_{v,a})s^-(h,\theta_{v,h},n_{v,h}).$$

We study numerically the response to different positioned perturbations in both systems which involve both geometries mentioned above. The initial condition corresponds to a trivial state ($u=1$ and $v=0$ in the Gray-Scott, and $u=0$ and $v=0$ in the MFN model). In both cases, a 16 by 16 mesh point area located over the semimajor (horizontal) axis was perturbed to $u=0.50$ and $v=0.25$. The systems suffer from the influence of a and h fields determined by the profile 1 (see Table I). Figures 12 and 13 show the patterns obtained from the Gray-Scott model and MFN model, respectively, on the elliptic geometry (for system response on the circular geometry, see Figs. 14 and 15). The horizontal position of perturbations was centered at 38.3, 42.3, 46.3, 50.3, and 54.3. The Gray-Scott parameter k ranges from 0.060 to 0.066, while the MFN parameter α_2 ranges from 0.0425 to 0.0725; both are uniformly spaced. Other adopted parameters are shown in Table IV. As we can see, for several values of the parameter k or α_2, the final patterns upon 2000 time steps depend strongly on the position where the perturbation occurs, while the geometry of the domain, either elliptical or circular, seems to have little influence in the case of the Gray-Scott model. However, in the MFN model, the patterns seem to be more sensitive to the shape of the surrounding tissue than in the Gray-Scott model, but less than for our model. It should be mentioned that, in contrast to the results discussed in the previous section, these patterns are not stable in the sense that they continue growing until all the domain is filled up.

IV. DISCUSSION

Early development of multicellular organisms is marked by a rapid increase in their cell numbers, accompanied by morphogenetic processes leading to the gradual formation of organs of characteristic shapes. During morphogenesis, through differentiation under strict genetic control, cells become more and more specialized. Further, genetic mechanisms such as morphogenesis also require generic physical principles, such as diffusion, spreading, differential adhesion, chemotaxis, etc. As a consequence, development relies on an intricate interplay of generic and genetic mechanisms. In this paper, we have addressed the issue of how chemical signaling derived from surrounding tissues can drive patterning processes. Our results, derived by computer simulation, suggest that the shape of the source (tissue) and other geometrical features strongly influence the formation of complex structures. In particular, we found that nonhomogeneous curvature of signaling tissues can generate complex patterns when acting on a gene network, while the same network embedded in a geometry with homogeneous curvature (boxes and circles) does not form localized structures. This result suggests an important consequence for development: let us consider that the shape of an organizer (tissue I or II in our case) is controlled by a gene network A, and the genic response to the organization field is controlled by a network B (the network shown in Fig. 3 in our case), which is not regulated by genes of network A. Any mutation in A that alters the shape of the organizer and consequently the organization field will affect the development of the induced structure or organ. Thus, we can conclude that biochemical interaction is not a necessary condition to explain alteration in the overall induced output; the interaction could be underlaid by a geometrical constraint imposed by the organizer. This conclusion is in agreement with the basis of epigenetic mechanisms for development proposed in previous studies [44,45].

In contrast to this hierarchic-type system, the self-organized systems examined here (Gray-Scott and MFN models) seem to be more insensitive to the gradients derived from surrounding tissues. However, this result does not seem to be general for all circumstances. In particular, Ref. [25] reports a Turing-type model in the morphodynamic perspective, which is sensitive to the geometry of the border of the studied domain.

Developmental mechanisms of patterning must be robust in order to ensure the functionality of organs, tissues, or coat patterns, under a wide range of environmental constraints and requirements. In organogenesis, signals produced at the wrong place or time can lead to an inappropriate developmental process, leading to a loss of the associated functions and/or to death. Thus, the robustness of patterns to noise becomes critical for the performance of the associated organ. Here, we have studied the robustness of patterns considering either the presence or absence of a positive feedback loop in the regulatory network. The two negative feedback loops presented in both cases were able to guarantee the stability of the pattern structure against a considerably high level of noise. However, the patterns driven by the first network seem to present higher robustness to noise than those generated by the second one. This example shows, as in many homeotic genes, that the positive feedback loop helps to foster the continuity of their expression, thus contributing to the stabilization of the patterns.

Although we have used a particular network topology with several mutually inhibiting factors, there are many other possibilities for the topology that could produce interesting patterns. Each topology can respond in a different way to the intrinsic noise of the patterning process. The particular case examined here was enough to conclude that the hierarchic-type mechanism, as the regulatory networks, can create complex biological shapes out of a simple structure. This mechanism could be enriched by incorporating geometrical constraints as key ingredients of morphogenesis processes.

ACKNOWLEDGMENTS

L.da F.C. is grateful to FAPESP (process 99/12765-2), CNPq (process 308231/03-1), and Human Frontier (RGP 39/2002) for financial support. L.D. thanks Human Frontier for Financial support.

[1] I. Salazar-Ciudad, J. Jernvall, and S. Newman, Development **130**, 2027 (2003).
[2] S. A. Newman, BioEssays **15**, 277 (1993).
[3] G. von Dassow, E. Meir, E. M. Munro, and G. M. Odell, Nature (London) **406**, 188 (2000).
[4] L. Diambra, L. C. Cintra, Q. Chen, D. Schubert, and L. da F. Costa, Physica A (to be published).
[5] M. Zajac, G. L. Jones, and J. A. Glazier, Phys. Rev. Lett. **85**, 2022 (2000).
[6] F. W. Cummings, J. Theor. Biol. **179**, 41 (1996).
[7] A. M. Turing, Philos. Trans. R. Soc. London, Ser. A **237**, 37 (1952).
[8] A. J. Koch and H. Meinhardt, Rev. Mod. Phys. **66**, 1481 (1994).
[9] K. J. Painter, P. K. Maini, and H. G. Othmer, Proc. Natl. Acad. Sci. U.S.A. **96**, 5549 (1999).
[10] J. B. Gurdon and P.-Y. Bourillot, Nature (London) **413**, 797 (2001).
[11] J. B. Gurdon, S. Dyson, and D. St. Johnston, Cell **95**, 159 (1998).
[12] D. E. Clyde, M. S. G. Corado, X. Wu, A. Paré A, D. Papatsenko, and S. Small, Nature (London) **426**, 849 (2003).
[13] P. W. Ingham, Nature (London) **335**, 25 (1988).
[14] N. A. M. Monk, Endeavour **24**, 170 (2000).
[15] L. Wolpert, R. Beddington, T. Jessel, P. Lawrence, E. Meyerowitz, and J. Smith, *Principles of Development* (Oxford University Press, Oxford, 2001).
[16] M. Freeman, Nature (London) **408**, 313 (2000).
[17] I. Salazar-Ciudad and J. Jernvall, Evol. Dev. **6**, 6 (2004).
[18] P. A. Wilson and A. Hemmati-Brivanlou, Nature (London) **376**, 331 (1995).
[19] M. Strigni and S. M. Cohen, Semin Cell Dev. Biol. **10**, 335 (1999).
[20] P. A. Wilson, G. Lagna, A. Susuki, and A. Hemmati-Brivanlou, Development **124**, 3177 (1997).
[21] Y. Miyazaki, Y. Nakanishi, and Y. Hieda, Dev. Dyn. **230**, 591 (2004).
[22] L. G. Harrison, S. Wehner, and D. M. Holloway, Faraday Discuss. **120**, 277 (2002).
[23] R. A. Barrio, P. K. Maini, J. L. Aragon, and M. Torres, Physica D **168**, 61 (2002).
[24] R. Plaza, F. Sanchez-Garduno, P. Padilla, R. A. Barrio, and P. K. Maini, J. Dyn. Differ. Equ. **16**, 1093 (2004).
[25] I. Salazar-Ciudad and J. Jernvall, Proc. Natl. Acad. Sci. U.S.A. **99**, 8116 (2002).
[26] R. Dillon and H. G. Othmer, J. Theor. Biol. **197**, 295 (1999).
[27] A. A. Teleman, M. Strigini, and M. S. Cohen, Cell **105**, 559 (2001).
[28] N. McDowell, J. B. Gurdon, and D. J. Grainger, Int. J. Dev. Biol. **45**, 199 (2001).
[29] E. V. Entchev, A. Schwabedissen, and M. Gonzalez-Gaitan, Cell **103**, 981 (2000).
[30] F. A. Ramirez-Weber and T. B. Kornberg, Cell **97**, 599 (1999).
[31] V. Greco, M. Hannus, and S. Eaton, Cell **106**, 633 (2001).
[32] J. Dubrulle, M. J. McGrew, and O. Pourquie, Cell **106**, 219 (2001).
[33] S. Y. Shvartsman, C. B. Muratov, and D. A. Lauffenburger, Development **129**, 2577 (2002).
[34] J. Reinitz and D. H. Sharp, Mech. Dev. **49**, 133 (1995).
[35] P. Smolen, P. E. Hardin, B. S. Lo, D. A. Baxter, and J. H. Byrne, Biophys. J. **86**, 2786 (2004).
[36] T. Mestl, E. Plahte, and S. W. Omholt, J. Theor. Biol. **176**, 291 (1995).
[37] C. W. Gardiner, *Handbook of Stochastic Methods: For Physics, Chemistry and the Natural Science* (Springer-Verlag, Berlin, 1985).
[38] See EPAPS Document No. E-PLEEE8-73-137603 for a movie showing the temporal evolution of patterning processes. The left panel corresponds to the temporal evolution of the pattern Fig. 7(b) during 800 steps. The right panel corresponds to the evolution in the same condition with the exception of pattern r_3 which changes from 32.02×10^{-2} to 32.1×10^{-2}. For more information on EPAPS, see http://www.aip.org/pubservs/epaps.html.
[39] A. Arkin, J. Ross, and H. H. McAdams, Genetics **149**, 1633 (1998).
[40] H. H. McAdams and A. Arkin, Proc. Natl. Acad. Sci. U.S.A. **94**, 814 (1997).
[41] P. Gray and S. K. Scott, J. Phys. Chem. **89**, 22 (1985).
[42] J. E. Pearson, Science **261**, 189 (1993).
[43] B. Vasiev, Phys. Lett. A **233**, 194 (2004).
[44] B. C. Goodwin, S. Kauffma, and J. D. Murray, J. Theor. Biol. **163**, 135 (1993).
[45] S. A. Newman and G. B. Müller, J. Exp. Zool. **288**, 304 (2000).